J. Fluid Mech. (1995), *vol.* 284, *pp.* 239–256

On coupling between the Poincaré equation and the heat equation: non-slip boundary condition

By K. ZHANG
Department of Mathematics, University of Exeter, Exeter EX4 4QJ, UK

(Received 19 January 1994 and in revised form 6 September 1994)

In contrast to the well-known columnar convection mode in rapidly rotating spherical fluid systems, the viscous dissipation of the preferred convection mode at sufficiently small Prandtl number Pr takes place only in the Ekman boundary layer. It follows that different types of velocity boundary condition lead to totally different forms of the asymptotic relationship between the Rayleigh number R and the Ekman number E for the onset of convection. We extend both perturbation and numerical analyses with the stress-free boundary condition (Zhang 1994) in rapidly rotating spherical systems to those with the non-slip boundary condition. Complete analytical solutions – the critical parameters for the onset of convection and the corresponding flow and temperature structure – are obtained and a new asymptotic relation between R and E is derived. While an explicit solution of the Ekman boundary-layer problem can be avoided by constructing a proper surface integral in the case of the stress-free boundary problem, an explicit solution of the spherical Ekman boundary layer is required and then obtained to derive the solvability condition for the present problem. In the corresponding numerical analysis, velocity and temperature are expanded in terms of spherical harmonics and Chebychev functions. Accurate numerical solutions are obtained in the asymptotic regime of small E and Pr, and comparison between the analytical and numerical solutions is then made to demonstrate that a satisfactory quantitative agreement between the analytical and numerical analyses is reached.

1. Introduction

The understanding of convective fluid motions in rapidly rotating fluid spherical systems is of fundamental importance to many problems in geophysics and planetary physics. There exist, in general, two distinctly different types of the convective motions: slowly drifting columnar rolls which are the most unstable for moderate or larger Prandtl numbers (Busse 1970; Zhang 1992) and fast azimuthally travelling waves in the form of an inertial mode of the Poincaré equation, which are preferred for smaller Prandtl numbers (Zhang 1994, hereinafter referred to as Z1). The connection between the Poincaré inertial modes and convective instabilities was discovered when the assumption of the stress-free boundary condition was made. Under this assumption, complete analytical solutions at the onset of convection in a rapidly rotating sphere were obtained on the basis of the perturbation of solutions of the Poincaré equation. While the assumption of the stress-free boundary condition is relevant to planetary fluid systems like atmospheres, and is mathematically convenient, it is inappropriate for systems like the liquid core of the Earth and for comparison with laboratory studies. In this section, we shall not attempt to discuss the relevant background and history of the subject, which can be found in previous papers (Zhang 1992; Z1) and

review articles, for example, by Fearn, Roberts & Soward (1988) and Proctor (1994). Instead, attention is focused on why the type of boundary condition is of central importance to the present problem.

The importance of the type of boundary condition for rotating spherical convection at small Prandtl numbers is connected with the most distinct and intriguing character of the Poincaré mode convection: the contribution of the viscous dissipation at the onset of convection comes solely from the Ekman boundary layer (Z1, equation (5.21)). As a consequence, the type of boundary condition plays an essential role in the analysis of the Poincaré mode convection, as contrasted with the well-known Roberts–Busse–Soward convection theory (Roberts 1968; Busse 1970; Soward 1977). For a better understanding of the present perturbation theory, it is worth comparing several key aspects of the present theory with Busse's perturbation theory (1970). For a rapidly rotating spherical system with a fixed rotation rate $\boldsymbol{\Omega}$, we may introduce an expansion in powers of a small parameter like the viscosity ν, and we assume that the zeroth order is in geostrophic balance (Busse 1970)

$$2\boldsymbol{\Omega}\times\boldsymbol{u}_0 = -\nabla P_0, \tag{1.1}$$

with boundary condition $\boldsymbol{u}_0\cdot\hat{r} = 0$, where (r,θ,ϕ) are spherical coordinates with unit vectors $(\hat{r},\hat{\theta},\hat{\phi})$. The only admissible solution of (1.1) is a steady azimuthal flow of the form

$$\boldsymbol{u}_0(\nu = 0) = \frac{1}{2|\boldsymbol{\Omega}|}\frac{\partial P_0}{\partial s}\hat{\phi}, \tag{1.2}$$

where (s,ϕ,z) are cylindrical coordinates with unit vectors $(\hat{s},\hat{\phi},\hat{z})$. The basic features of the solution of the zeroth-order problem (1.1) are thus fundamentally different from the corresponding convection solution

$$\boldsymbol{u}(\nu\to 0) = (u_s, u_\phi, u_z)\,\mathrm{e}^{\mathrm{i}m\phi+\mathrm{i}\omega t}, \tag{1.3}$$

which is obtained at arbitrarily small but non-zero ν. This represents a typical feature of a singular perturbation problem. In this case, the viscous dissipation of convective motions at leading order takes place only in the interior of the sphere and, consequently, there are no differences between the asymptotic laws (the relationship between the Rayleigh number R and the Ekman number E at the onset of convection) obtained from the stress-free and non-slip boundary conditions (Roberts 1968). However, if the zeroth-order equation is

$$\mathrm{i}\omega\boldsymbol{u}_0 + 2\boldsymbol{\Omega}\times\boldsymbol{u}_0 = -\nabla P_0, \tag{1.4}$$

which gives rise to a lower value of the Rayleigh number for the onset of convection at smaller Prandtl number Pr (Z1), an azimuthally travelling-wave solution of the form

$$\boldsymbol{u}_0(\nu = 0) = \boldsymbol{u}_0(s,z)\,\mathrm{e}^{\mathrm{i}m\phi+\mathrm{i}\omega t}, \tag{1.5}$$

is admitted. Solution (1.5) of the zeroth-order problem may smoothly approach the exact solution of convection for arbitrarily small but non-zero ν

$$\boldsymbol{u}(\nu\to 0)\to\boldsymbol{u}_0(\nu = 0),$$

except in the thin Ekman boundary layer. In this case, the viscous dissipation of convective motions at leading order takes place only in the Ekman boundary layer. The structure of the boundary layer is, of course, dependent upon the type of boundary

condition. It follows that different types of boundary condition lead to totally different forms of the asymptotic laws. From a mathematical point of view, the nature of the present analysis is regular perturbation while Busse's analysis (1970) is related to a singular perturbation problem. It should be noted that the complete boundaries that separate different convection modes in the $R-Pr$ parameter space cannot be determined by the present analysis, although we show that $R = O(E^{1/2})$ when $Pr \to 0$ (§3.3) and we know that $R = O(E^{-1/3})$ when $Pr \gg 1$ (Roberts 1968). This is due to the fact that a proper asymptotic theory for rotating spherical systems describing the spiralling convection mode, which is preferred at moderately small Prandtl number (Zhang 1992), is still not available, though a modification and an improvement for the Busse's annulus model was made by Yano (1992).

There exist a number of important differences between the stress-free and non-slip convection problems in rapidly rotating spherical fluid systems that are characterized by small Prandtl number. First, the non-slip boundary condition leads to an entirely new type of the asymptotic law for the Rayleigh number, because the amount of thermal energy needed to sustain the convective instability is solely determined by the structure of the Ekman boundary layer that is connected with the type of velocity boundary condition. Secondly, the effects of the spherical Ekman boundary layer in the case of the stress-free problem can be taken into account by constructing a proper surface integral and, consequently, a complicated spherical-boundary-layer solution is not needed. However, a complete solution of the spherical Ekman boundary layer is essential to the non-slip problem. This is because the stress-free boundary condition requires

$$\frac{\partial(u_\phi/r)}{\partial r} = \frac{\partial(u_\theta/r)}{\partial r} = 0, \tag{1.6}$$

and the viscous dissipation involves the second-order derivative $\partial^2/\partial r^2$. It follows that a surface integral that satisfies the first-order derivative condition (1.6) may be constructed from the solvability integrals (see Z1 for details) by partial integration. However, the non-slip boundary condition requires the disappearance of all velocity components at the boundaries without involving the radial derivative. As a result, the construction of a similar surface integral by partial integration to avoid an explicit boundary-layer solution is not possible. Thirdly, the leading-order solution is not modified in the case of the stress-free boundary condition. However, the leading-order solution for the non-slip problem is modified by the Ekman boundary-layer solution and, more importantly, the azimuthal symmetry of the convection cells of the leading-order solution is destroyed by the different azimuthal phases of the boundary-layer flow. Finally, a complete analytical expression for the critical Rayleigh number was obtained at the small Pr limit with the stress-free boundary condition, but the solvability integral associated with the Ekman boundary-layer solution for the non-slip problem must always be evaluated numerically. A nearly entirely new numerical code is needed for the non-slip problem because the spectral method is used for the numerical analysis. Moreover, obtaining a numerical solution for the non-slip problem characterized by a thin spherical Ekman boundary layer is much more difficult than for the corresponding stress-free problem.

The objectives of this paper are threefold. First, we extend the previous perturbation theory (Z1), which is based on the assumption of the stress-free boundary condition, to that for the non-slip boundary condition. Secondly, we carry out the numerical analysis of the same problem in the parameter space that is appropriate for comparing with the perturbation analysis. Thirdly, we compare the analytical solutions to the

numerical results and discuss relevant physical implications. Accordingly, the remainder of the paper is organized as follows. After giving the brief mathematical formulation of the problem in §2, the perturbation analysis is presented in §3. This is followed by the corresponding numerical analysis and discussion in §4 and closing remarks in §5.

2. Mathematical formulation

This section is kept brief since the mathematical formulation of the problem is similar to that described in Z1 (see also Chandrasekhar 1961). Consider the problem of linear convective instability in a Boussinesq rotating fluid spherical shell with constant thermal diffusivity κ, thermal expansion coefficient α, kinematic viscosity ν and gravity $\boldsymbol{g} = \gamma \boldsymbol{r}$, γ being a constant. The convective stability problem is governed by the following dimensionless equations:

$$\mathrm{i}\omega \boldsymbol{u} + 2\boldsymbol{k} \times \boldsymbol{u} = -\nabla P + R(1-\eta)^4 \Theta \boldsymbol{r} + E(1-\eta)^{-2} \nabla^2 \boldsymbol{u}, \tag{2.1}$$

$$\nabla \cdot \boldsymbol{u} = 0, \tag{2.2}$$

$$\left[\nabla^2 - \mathrm{i}\frac{Pr}{E}(1-\eta)^2 \omega\right] \Theta = -\boldsymbol{r} \cdot \boldsymbol{u}, \tag{2.3}$$

where $\boldsymbol{k}$ denotes the unit vector parallel to the rotation axis, $\boldsymbol{k} = \boldsymbol{\Omega}/|\boldsymbol{\Omega}|$, $\boldsymbol{r}$ is the position vector, η is r_i/r_o, the ratio of the radius of the inner sphere to that of the outer sphere, and Θ represents the temperature deviation from the purely conductive state, $\frac{1}{2}\beta r^2$, produced by a uniform distribution of heat sources (Chandrasekhar 1961). Equations (2.1)–(2.3) have been non-dimensionalized as follows

$$r \to (r_o - r_i) r, \quad t \to t(r_o - r_i)^2/\nu, \quad \Theta \to \Theta \beta (r_o - r_i)^2 \nu / \kappa.$$

The non-dimensional parameters – the modified Rayleigh number R, the Prandtl number Pr and the Ekman number E – are defined as

$$R = \frac{\alpha \beta \gamma r_o^4}{\Omega \kappa}, \quad Pr = \frac{\nu}{\kappa}, \quad E = \frac{\nu}{\Omega r_o^2}.$$

It should also be noted that the Rayleigh number R and frequency ω in (2.1)–(2.3) are rescaled by the Ekman number E. The velocity boundary conditions are non-slip and impenetrable, which give

$$u_\phi = u_\theta = u_r = 0 \tag{2.4}$$

at the inner and outer bounding spherical surfaces. Perfect thermally conducting boundaries impose

$$\Theta(r_i, \theta, \phi) = \Theta(r_o, \theta, \phi) = 0. \tag{2.5}$$

The type of thermal boundary condition for Θ is unlikely to be critically important since the temperature Θ does not enter into the leading-order problem. Note that the boundary conditions at $r = r_i$ apply only to the numerical solutions. The problem of convective instability is then defined by (2.1)–(2.3) with boundary conditions (2.4)–(2.5). Both numerical and analytical solutions to the same problem are sought. While a spherical shell ($\eta > 0$) is concerned in the numerical analysis, a full sphere ($\eta = 0$) is considered in the perturbation analysis.

3. Perturbation analysis

3.1. *Solvability condition*

For the perturbation approach of the convective instability problem, we assume that solutions of the problem for arbitrarily small but non-zero E can be written as

$$\boldsymbol{u} = \boldsymbol{u}_0 + (\boldsymbol{u}_b + \boldsymbol{u}_i), \quad P = P_0 + (P_i + P_b), \quad \omega = \omega_0 + \omega_1. \tag{3.1a–c}$$

Here $(\boldsymbol{u}_0, P_0, \omega_0)$ represent the inviscid solution when $E = 0$ with

$$\boldsymbol{u}_0 = O(1), \quad P_0 = O(1), \tag{3.2a}$$

$\boldsymbol{u}_i$ and P_i refer to the small interior perturbations to $(\boldsymbol{u}_0, P_0)$ when E is arbitrarily small but non-zero

$$\boldsymbol{u}_i = O(E^{1/2}), \quad P_i = O(E^{1/2}), \tag{3.2b}$$

$\boldsymbol{u}_b$ and P_b denote the boundary-layer correction introduced by the arbitrarily small but non-zero E and non-slip boundary condition (2.4)

$$\boldsymbol{u}_b = O(1), \quad P_b = O(1), \tag{3.2c}$$

which are non-zero only in the Ekman boundary layer of thickness $O(E^{1/2})$, and ω_1 is a small perturbation to ω_0. Substituting expansions (3.1*a*)–(3.1*c*) into equations (2.1)–(2.3), the leading order ($E = 0$) of the perturbation problem in the limit $\eta = 0$ gives rise to

$$\mathrm{i}\omega_0 \boldsymbol{u}_0 + 2\boldsymbol{k} \times \boldsymbol{u}_0 = -\nabla P_0, \tag{3.3}$$

$$\nabla \cdot \boldsymbol{u}_0 = 0, \tag{3.4}$$

together with impenetrable boundary condition $\boldsymbol{u}_0 \cdot \hat{r} = 0$ at $r = r_o$. In the limit $E = 0$, the other boundary conditions as well as heat equation (2.3) are not involved. Some special properties of equations (3.3)–(3.4) were discussed by Zhang (1993) and the precise form of the relevant solutions $\boldsymbol{u}_0$ was also given by equations (13)–(15) in the same paper.

When the Ekman number E is arbitrarily small but non-zero, governing equations at the next order perturbation problem for the whole sphere (including the interior perturbation and boundary correction) can be derived by substituting expansions (3.1*a*)–(3.1*c*) into equations (2.1)–(2.3) and subtracting equations (3.3)–(3.4)

$$\mathrm{i}\omega_o(\boldsymbol{u}_b + \boldsymbol{u}_i) + 2\boldsymbol{k} \times (\boldsymbol{u}_b + \boldsymbol{u}_i) + \nabla(P_i + P_b) = Ra\boldsymbol{r}\Theta + E\nabla^2(\boldsymbol{u}_0 + \boldsymbol{u}_b) - \mathrm{i}\omega_1(\boldsymbol{u}_0 + \boldsymbol{u}_b), \tag{3.5}$$

$$(\nabla^2 - \mathrm{i}\omega_o E^{-1} Pr)\,\Theta = -\boldsymbol{r} \cdot \boldsymbol{u}_0, \tag{3.6}$$

$$\nabla \cdot (\boldsymbol{u}_b + \boldsymbol{u}_i) = 0, \tag{3.7}$$

where smaller terms, $\mathrm{i}\boldsymbol{u}_i\omega_1$, $E\nabla^2\boldsymbol{u}_i$ and $\boldsymbol{r} \cdot \boldsymbol{u}_b = O(E^{1/2})$, are neglected. The boundary condition for $\boldsymbol{u}_b$ is

$$\hat{\phi} \cdot (\boldsymbol{u}_b - \boldsymbol{u}_0) = \hat{\theta} \cdot (\boldsymbol{u}_b - \boldsymbol{u}_0) = \hat{r} \cdot \boldsymbol{u}_b = 0 \tag{3.8}$$

at the outer spherical surface $r = r_o$. It is worth mentioning that the precise structure of $\boldsymbol{u}_i$ and how the boundary flow $\boldsymbol{u}_b$ is matched to the internal flow $\boldsymbol{u}_0$ at the edge of the boundary layer are of secondary significance for the present purpose of stability analysis.

The solvability conditions can be, as described in Z1, obtained by multiplying equation (3.5) by the complex conjugate of $\boldsymbol{u}_0$, denoted by $\boldsymbol{u}_0^*$, which also satisfies

$\nabla\cdot\boldsymbol{u}_0^*=0$ and boundary condition $\hat{r}\cdot\boldsymbol{u}_0^*=0$, and then by integrating over the volume of the sphere. The resulting left-hand side of equation (3.5) then vanishes because

$$\int_v \boldsymbol{u}_0^*\cdot[\mathrm{i}\omega_o(\boldsymbol{u}_b+\boldsymbol{u}_i)+2\boldsymbol{k}\times(\boldsymbol{u}_b+\boldsymbol{u}_i)+\nabla(P_i+P_b)]\,\mathrm{d}V$$

$$=\int_s \hat{r}\cdot[(\boldsymbol{u}_b+\boldsymbol{u}_i)P_0^*+\boldsymbol{u}_0^*(P_i+P_b)]\,\mathrm{d}S=0, \quad (3.9)$$

where P_0^* denotes the complex conjugate of P_0 and $\int_s \mathrm{d}S$ represents the surface integral over the spherical surface at $r=r_o$. The right-hand side of equation (3.5) then yields two integral equations, from its real and imaginary part:

$$\mathrm{Re}\left[R\int_v \boldsymbol{u}_0^*\cdot r\Theta\,\mathrm{d}V\right]=-\mathrm{Re}\left[E\int_v \boldsymbol{u}_0^*\cdot\nabla^2(\boldsymbol{u}_0+\boldsymbol{u}_b)\,\mathrm{d}V\right], \quad (3.10a)$$

and

$$\mathrm{Im}\left[R\int_v \boldsymbol{u}_0^*\cdot r\Theta\,\mathrm{d}V\right]=-\mathrm{Im}\left[E\int_v \boldsymbol{u}_0^*\cdot\nabla^2(\boldsymbol{u}_b+\boldsymbol{u}_0)\,\mathrm{d}V\right]+\omega_1\int_v |\boldsymbol{u}_0|^2\,\mathrm{d}V, \quad (3.10b)$$

where the term $\int_v \boldsymbol{u}_0^*\cdot\boldsymbol{u}_b\,\mathrm{d}V$ has been neglected compared with $\int_v |\boldsymbol{u}_0|^2\,\mathrm{d}V$ since $\boldsymbol{u}_b$ vanishes except in the Ekman boundary layer. Recognition of the fact that the velocity $\boldsymbol{u}_0^*$ is orthogonal to $\nabla^2\boldsymbol{u}_0$ (see Z1 for details)

$$\int_v \boldsymbol{u}_0^*\cdot\nabla^2\boldsymbol{u}_0\,\mathrm{d}V=0, \quad (3.11)$$

gives rise to

$$\mathrm{Re}\left[R\int_v \boldsymbol{u}_0^*\cdot r\Theta\,\mathrm{d}V\right]=-\mathrm{Re}\left[E\int_v \boldsymbol{u}_0^*\cdot\nabla^2\boldsymbol{u}_b\,\mathrm{d}V\right], \quad (3.12a)$$

$$\mathrm{Im}\left[R\int_v \boldsymbol{u}_0^*\cdot r\Theta\,\mathrm{d}V\right]=-\mathrm{Im}\left[E\int_v \boldsymbol{u}_0^*\cdot\nabla^2\boldsymbol{u}_b\,\mathrm{d}V\right]+\omega_1\int_v |\boldsymbol{u}_0|^2\,\mathrm{d}V. \quad (3.12b)$$

In other words, the contribution of the viscous dissipation comes only from the Ekman boundary layer. While equation (3.12*a*) determines the Rayleigh number for the onset of convection, equation (3.12*b*) calculates the correction for frequency ω_0 which is of less interest. Heat equation (3.6) is exactly the same, at leading order, as in the case of the stress-free boundary condition. The problem of linear convective instability in a rapidly rotating sphere with small Prandtl numbers can therefore be fully solved analytically if an explicit solution of the spherical Ekman boundary flow $\boldsymbol{u}_b$ is obtained.

It is also worth mentioning that the perturbation scheme with double expansion in terms of two small parameters – the Ekman number E and Prandtl number Pr – may be used for the present analysis, as treated by Busse (1983) for the problem of small-Prandtl-number convection. We have not adopted the double expansion approach for two reasons, which are also applicable to the previous analysis (Z1). First, there is no need to use the double expansion because Pr appears only in heat equation (3.6), and analytical solutions of equation (3.6) can be obtained for any parameters of E and Pr as shown in Z1. Secondly, without using the Prandtl number as an expansion parameter the dependence of our analytical solutions upon the Prandtl number Pr can be studied.

3.2. *Solutions of the spherical Ekman boundary layer*

The equation governing the Ekman boundary flow may be derived from (3.5). We first set the interior perturbation $\boldsymbol{u}_i=0$ and $P_i=0$, and then note that inside the Ekman boundary layer

$$|E\nabla^2\boldsymbol{u}_b|=O(1)\gg E\nabla^2\boldsymbol{u}_0, \quad |R\Theta|=O(RE^{1/2})\ll 1.$$

Making use of the above equations and neglecting the small term $i\omega_1(\boldsymbol{u}_0+\boldsymbol{u}_b)$ result in the order $O(1)$ equation for the Ekman boundary flow

$$i\omega_o \boldsymbol{u}_b + 2\boldsymbol{k}\times\boldsymbol{u}_b + \nabla P_b = E\nabla^2\boldsymbol{u}_b, \tag{3.13}$$

together with boundary condition

$$\boldsymbol{u}_b(1,\theta,\phi) = -(V_\theta\hat{\theta i} + V_\phi\hat{\phi})\exp(i(m\phi+\omega_0 t)) = -V\exp(i(m\phi+\omega_0 t))$$

at the outer spherical surface so that the total velocity is identically zero at the spherical surface $r = r_o$, where V_θ and V_ϕ are defined as

$$V_\theta = -\sin^{m-1}\theta\cos\theta(a_\theta\sin^2\theta + b\cos^2\theta + c), \tag{3.14}$$

$$V_\phi = \sin^{m-1}\theta(a_\phi\sin^2\theta + b\cos^2\theta + c). \tag{3.15}$$

Coefficients in (3.14)–(3.15) are given by

$$a_\phi = \frac{(2l-1)(2l+l\omega_0-2\omega_0)}{8(1-l)}, \quad a_\theta = \frac{(2l-1)(5l\omega_0-4\omega_0+2l-4)}{8(1-l)},$$

$$b = \frac{(2l-1)(l-2)\omega_0^2}{4(\omega_0-2)}, \quad c = \frac{(l-2)}{(2-\omega_0)},$$

where $l = m+2$ (see also Z1). For convenience, we may introduce a boundary-layer variable

$$\xi = E^{-1/2}(1-r), \quad \partial/\partial r = -E^{-1/2}\partial/\partial\xi.$$

To solve (3.13), first note that two independent equations can be deduced from (3.13)

$$\left(\frac{\partial^2}{\partial\xi^2} - i\omega_o\right)\hat{r}\times\boldsymbol{u}_b = -2(\boldsymbol{k}\cdot\hat{r})\boldsymbol{u}_b, \tag{3.16a}$$

$$\left(\frac{\partial^2}{\partial\xi^2} - i\omega_o\right)\boldsymbol{u}_b = 2(\boldsymbol{k}\cdot\hat{r})\hat{r}\times\boldsymbol{u}_b. \tag{3.16b}$$

Combining equations (3.16*a*) and (3.16*b*) gives a differential equation for $\boldsymbol{u}_b$

$$\left(\frac{\partial^2}{\partial\xi^2} - i\omega_o\right)^2\boldsymbol{u}_b + 4(\boldsymbol{k}\cdot\hat{r})^2\boldsymbol{u}_b = 0. \tag{3.17}$$

The velocity boundary condition at the outer spherical surface becomes

$$\boldsymbol{u}_b(\xi=0) = -V\exp(im\phi + i\omega_0 t), \tag{3.18a}$$

$$\frac{\partial^2\boldsymbol{u}_b}{\partial\xi^2}(\xi=0) = [-i\omega_o V - 2(\boldsymbol{k}\cdot\hat{r})\hat{r}\times V]\exp(im\phi + i\omega_0 t), \tag{3.18b}$$

while the condition that the boundary-layer flow must remain bounded gives

$$\boldsymbol{u}_b(\xi=\infty) = 0, \quad \frac{\partial^2\boldsymbol{u}_b}{\partial\xi^2}(\xi=\infty) = 0. \tag{3.19a, b}$$

In writing the conditions (3.18*b*) and (3.19*b*), we have used (3.16*b*). The fourth-order differential equation (3.17) together with the four boundary conditions (3.18*a*, *b*) and (3.19*a*, *b*) determines the relevant solution of the spherical Ekman boundary-layer problem.

It is straightforward to show that the solution of boundary-layer equation (3.17) satisfying boundary conditions (3.19*a*, *b*) is

$$\boldsymbol{u}_b = \left[C_1 \exp\left\{ \frac{-(1+S_1\,\mathrm{i})}{\sqrt{2}} |\omega_0 - 2\boldsymbol{k}\cdot\hat{\boldsymbol{r}}|^{1/2}\,\xi \right\} + C_2 \exp\left\{ \frac{-(1+S_2\,\mathrm{i})}{\sqrt{2}} |\omega_0 + 2\boldsymbol{k}\cdot\hat{\boldsymbol{r}}|^{1/2}\,\xi \right\} \right] \exp(\mathrm{i}m\phi + \mathrm{i}\omega_0 t), \quad (3.20)$$

where

$$S_1 = \frac{\omega_0 - 2\boldsymbol{k}\cdot\hat{\boldsymbol{r}}}{|\omega_0 - 2\boldsymbol{k}\cdot\hat{\boldsymbol{r}}|}, \quad S_2 = \frac{\omega_0 + 2\boldsymbol{k}\cdot\hat{\boldsymbol{r}}}{|\omega_0 + 2\boldsymbol{k}\cdot\hat{\boldsymbol{r}}|}.$$

Here C_1 and C_2, a function of θ and m, are complex vectors. For determining C_1 and C_2, we need the other two boundary conditions (3.18*a*, *b*) at the spherical surface $\xi = 0$, which yield

$$-V = C_1 + C_2,$$
$$-[\mathrm{i}\omega_o V + 2(\boldsymbol{k}\cdot\hat{\boldsymbol{r}})\hat{\boldsymbol{r}}\times V] = \mathrm{i}C_1(\omega_0 - 2\boldsymbol{k}\cdot\hat{\boldsymbol{r}}) + \mathrm{i}C_2(\omega_0 + 2\boldsymbol{k}\cdot\hat{\boldsymbol{r}}),$$

which have the following solution

$$C_1 = -\tfrac{1}{2}(V + \mathrm{i}\hat{\boldsymbol{r}}\times V), \quad C_2 = -\tfrac{1}{2}(V - \mathrm{i}\hat{\boldsymbol{r}}\times V).$$

On substituting the complex vectors, C_1 and C_2, into (3.20), we obtain the required solution of the spherical Ekman boundary layer

$$\boldsymbol{u}_b = -\frac{1}{2}\left[(V + \mathrm{i}\hat{\boldsymbol{r}}\times V) \exp\left\{ \frac{-(1+S_1\,\mathrm{i})}{\sqrt{2}} |\omega_0 - 2\boldsymbol{k}\cdot\hat{\boldsymbol{r}}|^{1/2} E^{-1/2}(1-r) \right\} + (V - \mathrm{i}\hat{\boldsymbol{r}}\times V) \exp\left\{ \frac{-(1+S_2\,\mathrm{i})}{\sqrt{2}} |\omega_0 + 2\boldsymbol{k}\cdot\hat{\boldsymbol{r}}|^{1/2} E^{-1/2}(1-r) \right\} \right] \exp(\mathrm{i}m\phi + \mathrm{i}\omega_0 t). \quad (3.21)$$

It should be noted that the boundary correction owing to the radial flow is of the order $E^{1/2}$ (Greenspan 1968) and is therefore not included. It should also be pointed out that boundary solution (3.21) breaks down at the critical latitude $\theta_c = \cos^{-1}(\frac{1}{2}\omega_0)$. A substantial effect of the singular circle at θ_c, however, is not anticipated, as confirmed by the numerical analysis in §4, since the amplitude of the equatorially trapped mode decreases nearly exponentially from the equator and the gradient of velocity at the critical latitude is fairly weak (Zhang 1993).

3.3. *Analytical results for the onset of convection*

Substitution of solution (3.20) of the Ekman boundary-layer problem into equations (3.12*a*) and (3.12*b*) gives rise to the Rayleigh number R and the correction for frequency ω_1 at the onset of convection

$$R = \frac{2\pi E^{1/2}}{\sqrt{2}\,\mathrm{Re}[H_\Theta]} \int_0^\pi \sin\theta([V_\phi]^2 + [V_\theta]^2)\,|\omega_0 - 2\cos\theta|^{1/2}\,\mathrm{d}\theta, \quad (3.22a)$$

$$\omega_1 = \left\{ \mathrm{Im}[H_\Theta]\,R - \frac{2\pi E^{1/2}}{\sqrt{2}} \int_0^\pi S_1 \sin\theta([V_\phi]^2 + [V_\theta]^2)\,|\omega_0 - 2\cos\theta|^{1/2}\,\mathrm{d}\theta \right\} \Big/ \int_v |\boldsymbol{u}_0|^2\,\mathrm{d}V \quad (3.22b)$$

where

$$H_\Theta = \int_v \boldsymbol{u}_0^* \cdot \boldsymbol{r}\Theta\,\mathrm{d}V,$$

which is not affected by the non-slip boundary condition at leading order. In writing expressions (3.22*a*, *b*), we have neglected the following integral

$$I_a = \int_0^\pi \mathrm{i} V^* \cdot (\hat{r} \times V) |\omega_0 - 2\cos\theta|^{1/2} \sin\theta \, \mathrm{d}\theta.$$

This is based on the fact that the function $\mathrm{i}V^* \cdot (\hat{r} \times V)$ is equatorially anti-symmetric

$$\mathrm{i}V^* \cdot (\hat{r} \times V)(\theta) = -\mathrm{i}V^* \cdot (\hat{r} \times V)(\pi - \theta),$$

but the function $|\omega_0 - 2\cos\theta|$ is nearly equatorially symmetric. The inclusion of I_a in expressions (3.22*a*, *b*), as has been checked, does not produce a significant change in the result.

Let us first consider the simplest case when the thermal diffusion term in heat equation (3.6) is dominant

$$|\nabla^2 \Theta| \gg \left| \frac{Pr}{E} \omega_0 \Theta \right|,$$

where $\omega_0 = O(m^{-1/2})$ (Z1) and $|\nabla^2 \Theta| = O(m^2 \Theta)$, which leads to $Pr\, m^{-5/2} \ll E$. In this case, the term $\partial\Theta/\partial t$ may be neglected and an analytical solution for heat equation (3.6) in the closed form can be obtained to give

$$\begin{aligned} \mathrm{Re}[H_\Theta] = {} & E_6 I_{l+1,0} + E_4 I_{l-1,2} + E_3 I_{l,0} + E_5 I_{l,1} + E_2 I_{l-1,1} \\ & + E_1 I_{l-1,0} + E_7 I_{l-2,1} + E_8 I_{l-2,2} + E_9 I_{l-2,0} + E_{10} I_{l-2,3}, \quad (3.23a) \\ \mathrm{Im}[H_\Theta] = {} & 0, \quad (3.23b) \end{aligned}$$

where $I_{n,j}$ is defined as

$$I_{n,j} = \frac{2^{n+2} \pi n! (2j-1)!!}{(2n+2j+3)!!},$$

and the coefficients $\{E_k, k = 1, 2, \ldots, 10\}$ have explicit analytical expressions (see Z1 for details). For a general expression that is valid for any values of Pr and E, we have the following analytical formulae

$$\mathrm{Re}[H_\Theta] = \sum_{l=m}^{m+2} \sum_{n=1}^{N} \frac{[a_s Z_{ln}^1 + (d+b) Z_{ln}^2 + c B_{ln}^2 Z_{ln}^3]^2}{B_{ln}^{2m+8} j_{l+1}^2(B_{ln}) [Pr^2 E^{-2} \omega^2 + B_{ln}^4]}, \quad (3.24)$$

$$\mathrm{Im}[H_\Theta] = \sum_{l=m}^{m+2} \sum_{n=1}^{N} \frac{-(\omega_0 E^{-1} Pr)[a_s Z_{ln}^1 + (d+b) Z_{ln}^2 + c B_{ln}^2 Z_{ln}^3]^2}{B_{ln}^{2m+10} j_{l+1}^2(B_{ln}) [Pr^2 E^{-2} \omega^2 + B_{ln}^4]}. \quad (3.25)$$

Here Z_{ln}^1, Z_{ln}^2, Z_{ln}^3, a_s, b, c and d are again analytical functions of wavenumber m and ω_0, their detailed expressions are given in Z1 and $j_l(B_{ln})$ satisfies

$$j_l(B_{ln}) = 0, \quad 0 < B_{l1} < B_{l2} < B_{l3} < \ldots,$$

where $j_l(x)$ is the spherical Bessel function. Note also that the $l = m+1$ term in the sum $\sum_{l=m}^{m+2}$ is zero and, hence, should not be included in equations (3.24) and (3.25). The value of N is chosen according to the desired accuracy and four terms ($N = 4$) can usually give a better than 1 % accuracy of approximation.

The general Rayleigh number expression (3.22*a*) is rather complicated, but a case of mathematical interest and much less complex is the zero Prandtl number limit. In this limit, H_Θ is real and independent of E and Pr, and the Rayleigh number R at the onset of convection, according to formula (3.22*a*), obeys an asymptotic law

$$R \sim E^{1/2}.$$

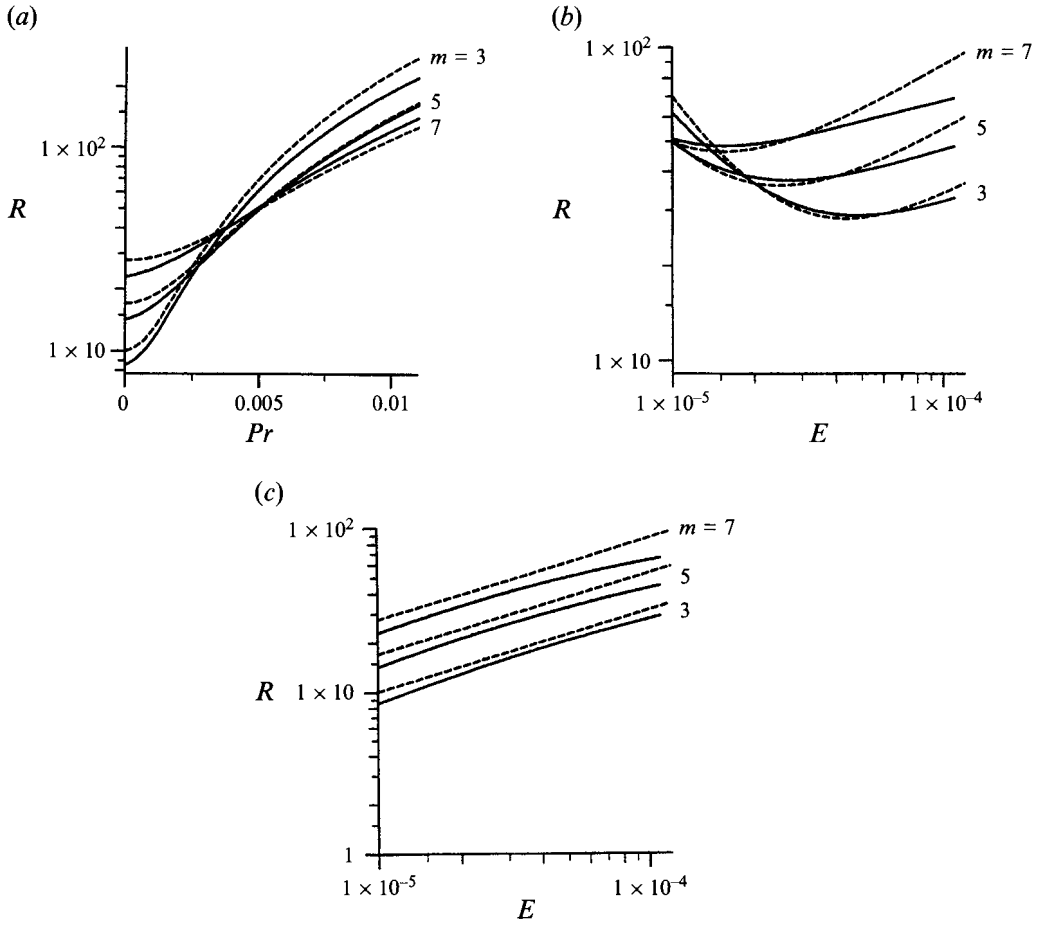

FIGURE 1. (*a*) The Rayleigh number R plotted against the Prandtl number Pr for wavenumbers $m = 3, 5, 7$. The Rayleigh number shown as a function of the Ekman number E, (*b*) for $Pr = 0.005$ and (*c*) for $Pr = 0$. ——, Numerical results; – – –, analytical results.

This is to be contrasted with the asymptotic law (Roberts 1968; Busse 1970) for the columnar convection, in which the Rayleigh number R increases rapidly with decreasing Ekman number

$$R \sim E^{-1/3},$$

where the difference between the definitions of the Rayleigh number has been taken into account. The precise relationship $R \sim E^{1/2}$ at the limit $Pr = 0$ calculated from expression (3.22*a*) and (3.23) is presented in figure 1(*c*) for three different azimuthal wavenumbers; the corresponding numerical results with an inner sphere $\eta = 0.2$ are also shown in the same figure which will be discussed in §4. Only odd wavenumbers are presented in the figure since the inclusion of both even and odd wavenumbers does not yield any new physics, but gives too many curves resulting in an unclear picture. Such a simple power-law dependence is, however, not expected when the condition $Pr \ll Em^{-5/2}$ is not satisfied. This is because of the factor $E^{-2}Pr^2$ appearing in the analytical expression (3.24). Dependence of R upon E for the three different wavenumbers based on expressions (3.22*a*) and (3.24) is displayed in figure 1(*b*) for $Pr = 0.005$, and the corresponding Rayleigh number dependence on the Prandtl number Pr at $E = 10^{-5}$ is

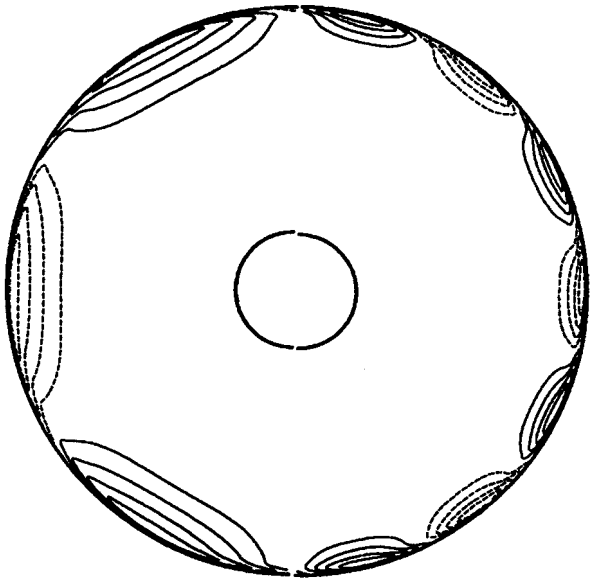

FIGURE 2. Contours of u_ϕ obtained from analytical formula (3.26) with $m = 7$ on the left-hand side and $m = 3$ on the right-hand side at the equatorial plane.

shown in figure 1(*a*). For $E = 10^{-5}$, the most unstable wavenumber m_c is 3 at $Pr = 0$, which is increased to $m_c = 5$ at $Pr = 0.003$ and becomes $m_c = 7$ at $Pr = 0.006$. In general, the Rayleigh number and the most unstable wavenumber increase with increasing Prandtl number.

An important and interesting feature concerning the structure of convection for the non-slip boundary condition is the phase modulation of the convection cell, which destroys the azimuthal symmetry of a cell with the stress-free boundary condition (figure 4, Z1) described by $\cos m\phi$. The total convection velocity in the whole sphere at leading order may be written as

$$u_\phi = [a_\phi r^{m+1} \sin^{m+1}\theta + br^{m+1}\sin^{m-1}\theta\cos^2\theta + cr^{m-1}\sin^{m-1}\theta + \hat{\phi}\cdot\boldsymbol{F}]\exp(\mathrm{i}(m\phi+\omega_0 t)), \tag{3.26}$$

$$u_\theta = [a_\theta r^{m+1} \sin^{m+1}\theta + br^{m+1}\sin^{m-1}\theta\cos^2\theta + cr^{m-1}\sin^{m-1}\theta + \hat{\theta}\cdot\boldsymbol{F}]\exp(\mathrm{i}(m\phi+\omega_0 t)), \tag{3.27}$$

where

$$\boldsymbol{F} = -0.5[(\boldsymbol{V}+\mathrm{i}\hat{r}\times\boldsymbol{V})\exp(-(2E)^{-1/2}(1+S_1\mathrm{i})|\omega_0-2\cos\theta|^{1/2}(1-r)) + (\boldsymbol{V}-\mathrm{i}\hat{r}\times\boldsymbol{V})\exp(-(2E)^{-1/2}(1+S_2\mathrm{i})|\omega_0+2\cos\theta|^{1/2}(1-r))].$$

Note that u_r is the same as the radial component of $\boldsymbol{u}_0$ at leading order. The phase modulation on the interior convection cell by the Ekman boundary flow is suggested by the complex vector $\boldsymbol{F}$. Contours of u_ϕ calculated from formula (3.26) are displayed in figure 2 for two different cases. Similar phase modulation is also found in numerical solutions. We have not shown the profile of temperature Θ since it is almost identical to that of the numerical solution which is not affected by the non-slip boundary condition at leading order. A small perturbation to the frequency ω_0 is of secondary significance for the problem of convective instability. However, it can be seen from (3.22*b*) that the frequency ω_0 is always reduced by the thermal effects.

4. Numerical analysis

4.1. *Numerical method*

For the convenience of numerical analysis, we expand the solenoidal velocity $\boldsymbol{u}$ in the poloidal and toroidal decomposition

$$\boldsymbol{u} = \nabla \times \nabla \times r v + \nabla \times r w. \tag{4.1}$$

Boundary condition (2.4) at the inner and outer bounding spherical surfaces then becomes

$$v = \frac{\partial v}{\partial r} = w = 0. \tag{4.2}$$

The poloidal and toroidal fields, v and w, and the temperature deviation, Θ, are then expanded in terms of spherical harmonics $Y_l^m(\theta, \phi)$ and Chebychev functions $T_l(x)$ with the factor $(1-x^2)$ which is retained to satisfy boundary conditions (2.4) and (2.5)

$$\Theta = (1-x^2) \sum_{l,n} \Theta_{lmn}\, T_{n-1}(x)\, Y_l^m(\theta, \phi)\, \mathrm{e}^{\mathrm{i}\omega t}, \tag{4.3}$$

$$v = (1-x^2)^2 \sum_{l,n} v_{lmn}\, T_{n-1}(x)\, Y_l^m(\theta, \phi)\, \mathrm{e}^{\mathrm{i}\omega t}, \tag{4.4}$$

$$w = (1-x^2) \sum_{l,n} w_{lmn}\, T_{n-1}(x)\, Y_l^m(\theta, \phi)\, \mathrm{e}^{\mathrm{i}\omega t}, \tag{4.5}$$

where coefficients Θ_{lmn}, v_{lmn} and w_{lmn} are complex and time independent, m is the azimuthal wavenumber and

$$x = 2r - (1+\eta)/(1-\eta).$$

The $Y_l^m(\theta, \phi)$ are normalized such that the spherical surface integral

$$\frac{1}{4\pi} \int_S |Y_l^m(\theta, \phi)|^2 \sin\theta \, \mathrm{d}\theta \, \mathrm{d}\phi = 1. \tag{4.6}$$

For a given set of parameters, E, Pr and m, the subsequent procedure for obtaining the Rayleigh number R, the frequency ω and complex coefficients Θ_{lmn}, v_{lmn} and w_{lmn} at the onset of convection is the same as described in Z1 (see also Zhang & Busse 1987). However, an almost entirely new computational code is needed because the Galerkin spectral method is used.

4.2. *Numerical results for the onset of convection*

It is of vital importance that numerical solutions are capable of resolving the thin Ekman boundary layer arising from the non-slip boundary condition in order that a proper comparison between a numerical and an analytical solution can be made. The accuracy of numerical solutions was therefore carefully checked at different regions of the parameter space. Table 1 illustrates two examples of convergence of the numerical solutions for the parameters $\eta = 0.2$, $E = 10^{-5}$ and $Pr = 0.001$, which are the most demanding cases in this paper as far as numerical resolution is concerned. It is also worth mentioning that satisfactory convergence is not only demonstrated by the critical parameters for the onset of convection, but also confirmed by the same detailed structure of the numerical solutions at different levels of the truncation. The choice of Chebyshev functions appears to lead to a quite satisfactory accuracy. Throughout the paper the value of the truncation parameter N_t is always chosen in accordance with the parameters of solutions to secure better than 2% accuracy.

An interesting case for both numerical and analytical analysis is the simplest asymptotic relation $R \sim E^{1/2}$, predicted by analytical formula (3.22a) in the small Prandtl number limit $Pr \ll Em^{-5/2}$. This power-law dependence is clearly borne out in

	$m = 3$		$m = 7$	
N_t	R	ω	R	ω
20	11.7	−0.242	25.5	−0.245
24	11.3	−0.242	25.0	−0.245
26	11.3	−0.242	25.1	−0.245
28	11.3	−0.242	25.4	−0.245
30	11.4	−0.242	25.1	−0.245

TABLE 1. Examples of the convergence behaviour for $E = 10^{-5}$ and $Pr = 0.001$ with $\eta = r_i/r_o = 0.2$.

the numerical analysis which is displayed in figure 1(*c*) for $Pr = 0$ together with the corresponding analytical results, though the analytical formula appears to overestimate the values of the Rayleigh number. A further case is when the effects of the Prandtl number are substantial: $Pr \ll Em^{-5/2}$. This is illustrated in figure 1(*b*) by a typical case with $Pr = 0.005$. There seems no simple power-law dependence between R and E for this case, as suggested by the factor of $(E^{-1}Pr)^2$ in analytical formula (3.24). While the numerical curves depart significantly from the analytical curves for the larger Ekman numbers $E > 5 \times 10^{-5}$, the differences between the analytical and numerical curves are less noticeable for the smaller Ekman numbers, $E < 5 \times 10^{-5}$. A typical dependence of the Rayleigh number R upon the Prandtl number Pr, again together with the analytical results, is shown in figure 1(*a*). It can be seen that the values of the Rayleigh number R and the most unstable wavenumber m_c increase, in general, with increasing Prandtl number Pr and that the agreement between our analytical and numerical analysis is again reasonably satisfactory. The differences between the predicted values of R by (3.22*a*) and the corresponding numerical values are insignificant, and the analytically predicted most unstable wavenumber m_c, which is associated with the minimum value of R calculated by using expression (3.22*a*), is exactly the same as that determined by the corresponding numerical solutions.

An important question that deserves a physical explanation is why the most unstable mode is switched from a columnar spiralling mode (Zhang 1992) to an equatorially trapped Poincaré mode described in this paper. An explanation may be partially provided by contrasting the two distinct convection solutions obtained at exactly the same parameters ($E = 10^{-5}, Pr = 0.005, m = 5$) which are shown in figure 3. The transition of the preferred form, from the spiralling mode to the Poincaré mode, occurs at $0.005 < Pr < 0.01$ for $E = 10^{-5}$. While the Rayleigh number is $R = 49.0$ with $\omega = 0.24$ for the Poincaré mode at $Pr = 0.005$, the Rayleigh number for the spiralling mode is $R = 54.0$ with $\omega = 0.12$. It is suggested that the switch-over from the spiralling mode to the Poincaré mode may be interpreted as being a consequence of two competitive ways of transporting heat by convection. With decreasing Prandtl number, the columnar convection roll is increasingly extended and stretched in the direction of rotation (eastward), and the stretching is so enormous that the radial scale becomes eventually shorter in comparison with the azimuthal scale. This leads to a sharp increase of the viscous dissipation and to the reduction of effectiveness of the radial heat transport by convection. The Poincaré mode provides an alternative form of convection in which the Coriolis forces are primarily balanced by the inertial and pressure forces and heat transport is concentrated in the equatorial region.

It should be pointed out that our numerical solutions with the expansion of radial functions by (4.3–4.5) break down at $\eta = 0$. All numerical results shown in figure 1 are

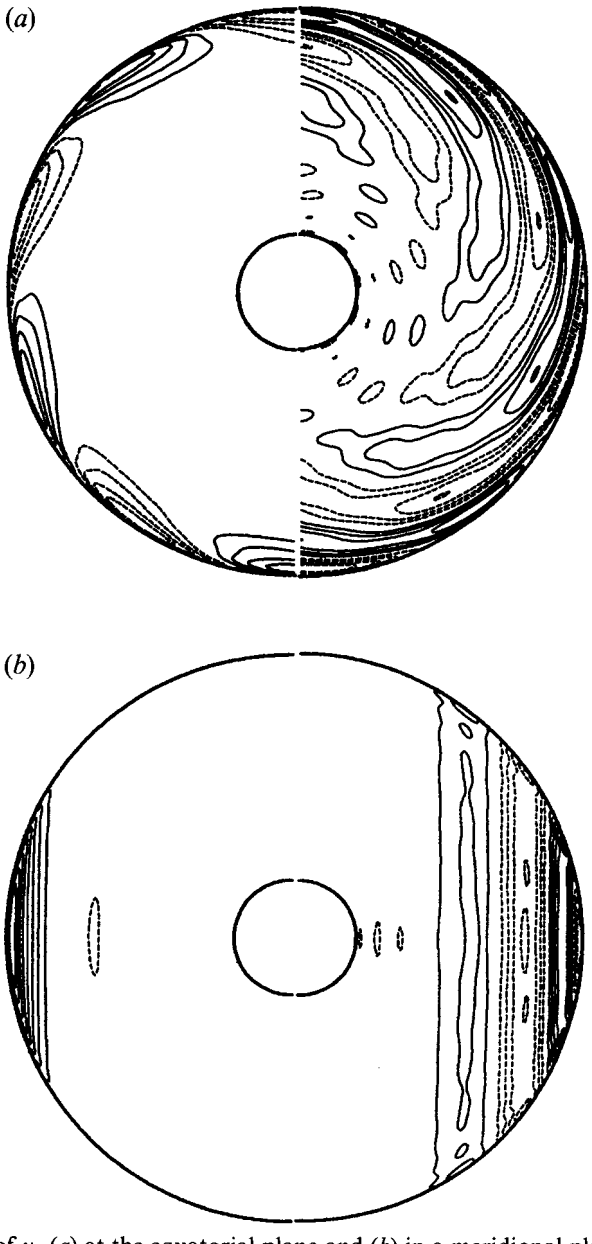

FIGURE 3. Contours of u_ϕ (*a*) at the equatorial plane and (*b*) in a meridional plane. On the left-hand side is the Poincaré convection mode and on the right-hand side is the spiralling columnar mode. Both are obtained at the same Ekman and Prandtl numbers with $E = 10^{-5}$, $Pr = 0.005$ and $m = 5$.

thus computed at $\eta = 0.2$, which is small enough to compare with the analytical solutions of a sphere and at the same time, large enough to obtain rapidly convergent numerical solutions. With regard to the application of the present theory for a sphere to planetary systems, however, it is of importance to understand the effects of an inner core, which cannot be understood on the basis of the available analytical solutions. Two typical examples of numerical convection solutions, one with a large scale with $m = 3$ and another with a smaller scale with $m = 7$, are shown in table 2. The corresponding structures of convection at $\eta = 0.2$ and 0.5 are shown in figure 4 for

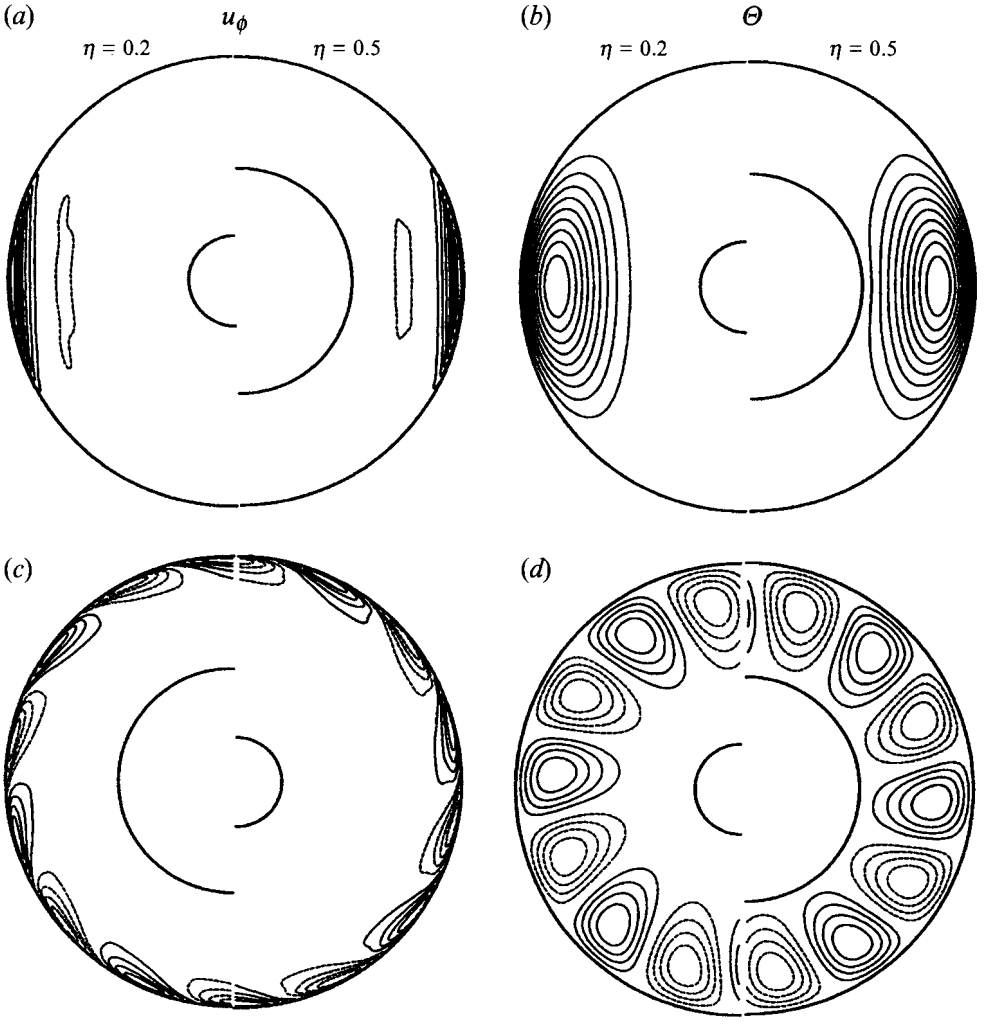

FIGURE 4. (*a*) Contours of u_ϕ and (*b*) contours of Θ in a meridional plane, (*c*) contours of u_ϕ and (*d*) contours of Θ at the equatorial plane for $Pr = 0.001$ and $E = 10^{-5}$ with $m = 7$. On the left-hand side is for the smaller inner sphere with $\eta = 0.2$ while the case of $\eta = 0.5$ is on the right-hand side.

	$\eta = 0.2$		$\eta = 0.3$		$\eta = 0.4$		$\eta = 0.5$	
	R	ω	R	ω	R	ω	R	ω
$m = 3$	11.4	−0.242	12.6	−0.240	15.6	−0.235	23.0	−0.222
$m = 7$	25.1	−0.245	25.8	−0.245	26.5	−0.245	27.6	−0.245

TABLE 2. The Rayleigh numbers and frequencies obtained for different sizes of the inner sphere at $E = 10^{-5}$ and $Pr = 0.001$.

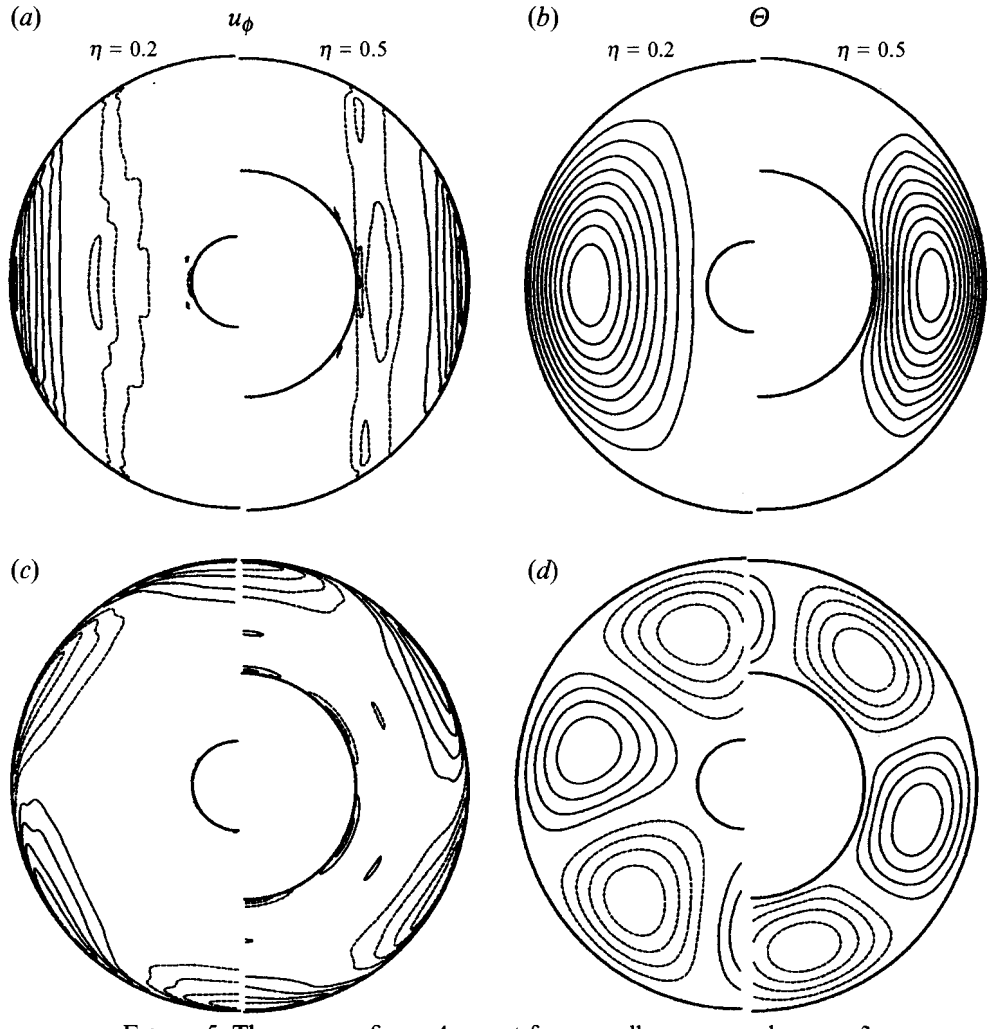

FIGURE 5. The same as figure 4 except for a smaller wavenumber $m = 3$.

$m = 7$ and in figure 5 for $m = 3$. General behaviour appears to be associated with the formula (Zhang 1993),

$$m_s = \frac{\pi(1+\eta)}{2(1-\eta)}.$$

When $m \geqslant m_s$, convection is insignificantly affected by the presence of an inner sphere. For the smaller scale convection with $m = 7$, which is mainly localized in the equatorial region, there are very few noticeable effects on the structure resulting from the presence of an inner sphere even with $\eta = 0.5$, as displayed in figure 4. The Rayleigh number R obtained from the numerical solutions increases slightly from $R = 25.1$ at $\eta = 0.2$ to $R = 27.6$ at $\eta = 0.5$. By contrast, the Rayleigh number R increases sharply for the larger scale convection with $m = 3$, from $R = 11.4$ at $\eta = 0.2$ to $R = 23.0$ at $\eta = 0.5$. An explanation for this sharp increase can readily be provided from the structure of convection illustrated in figure 5 and its comparison to figure 4. In addition to the Ekman boundary layer at the outer spherical surface, the non-axisymmetric Stewartson-type layer (Stewartson 1966) attaching the equator of the inner sphere is formed when the size of the inner sphere and the scale of flow are too large, resulting

in an extra viscous dissipation. In consequence, the Rayleigh number R is much larger. It is therefore inappropriate to apply the present perturbation theory of a sphere described in §3 to the cases which are characterized by a large-scale flow or a large inner sphere which may lead to wavenumber $m < m_s$. For the case of the Earth's fluid core with $\eta \approx 0.35$, the present analytical theory would give rise to a fairly accurate solution if the wavenumber of convection $m \geqslant 3$, equivalent to a typical flow scale smaller than 3000 km.

5. Concluding remarks

For the convection problem in a rotating system, the Prandtl number Pr is a key parameter and enters into the problem from its first instability, which can be contrasted with the case of non-rotating convection. Many planetary and astrophysical fluids are characterized by rapid rotation and small Prandtl numbers. Moreover, it is reasonable to anticipate that the effective Prandtl numbers may be even smaller owing to the radiative contribution to the thermal diffusivity in the atmospheres of the major planets and Earth's outer core. Convection in the form of inertial waves may have a direct relevance to the dynamics of the Earth's fluid core. The existence of the inertial waves was observed in the laboratory experiment by Aldridge & Toomre (1969) and identified by the gravity observation on the Earth's surface by Aldridge & Lumb (1987). However, the mechanism of exciting and sustaining these inertial waves in the Earth's outer core remains unclear. Kerswell has (1994*a*, *b*) studied the possibility of exciting the inertial waves by the mechanism of an elliptical instability in a tidally distorted rotating spheroid. The mathematical difficulties in the understanding of the inertial waves in the Earth's outer core are mainly associated with the possibility of a continuous wave spectrum and the mechanism of selecting and sustaining an inertial wave. These difficulties can be readily overcome within the framework of instability theory described in this paper. On the assumptions that an inertial wave is excited and maintained by convective instability and that the physically observed inertial mode always corresponds to the most unstable mode, the problem of inertial waves in the Earth's outer core may be understood on the basis of the present theory.

We have extended convective instability analysis for the Poincaré convection mode in rotating spherical systems from the case of the stress-free boundary condition to that of the non-slip boundary condition. An interesting and important question that remains to be answered is the behaviour of finite-amplitude solutions of the Poincaré convection mode. Investigation including weakly nonlinear effects of the system seems to be feasible because of the availability of the analytical linear convection mode, though the presence of the Ekman boundary layer may complicate the analysis. It is of particular interest to find out whether and how the Poincaré mode convection becomes unstable at finite amplitudes, and, if unstable, what the form of the corresponding secondary convection is. Another interesting question is in connection with the Poincaré equations in a rotating spherical shell. Numerical analysis in this paper indicates that the perturbation theory of a sphere can be applied to the case of a spherical shell if the wavenumber of convection $m > m_s$. A full understanding of the effects of an inner sphere on convection, however, requires a rigorous analysis involving analytical non-axisymmetric solutions of the Poincaré equation in a rotating spherical shell which are still not available (Greenspan 1968; Aldridge 1972).

REFERENCES

ALDRIDGE, K. D. 1972 Axisymmetric oscillations of a fluid in a rotating spherical shell. *Mathematika* **19**, 163–168.

ALDRIDGE, K. D. & LUMB, L. I. 1987 Inertial waves identified in the Earth's fluid outer core. *Nature* **325**, 421–423.

ALDRIDGE, K. D. & TOOMRE, A. 1969 Axisymmetric inertial oscillations of a fluid in a rotating spherical container. *J. Fluid Mech.* **37**, 307–323.

BUSSE, F. H. 1970 Thermal instabilities in rapidly rotating systems. *J. Fluid Mech.* **44**, 441–460.

BUSSE, F. H. 1983 A model of mean flows in the major planets. *Geophys. Astrophys. Fluid Dyn.* **23**, 152–174.

CHANDRASEKHAR, S. 1961 *Hydrodynamic and Hydromagnetic Stability*. Clarendon.

FEARN, D. R., ROBERTS, P. H. & SOWARD, A. M. 1988 Convection, stability and the dynamo. In *Energy, Stability and Convection* (ed. B. Straughan & P. Galdi), pp. 60–324. Longman.

GREENSPAN, H. P. 1968 *The Theory of Rotating-Fluids*. Cambridge University Press.

KERSWELL, R. R. 1994*a* Tidal excitation of hydromagnetic waves and their damping in the Earth. *J. Fluid Mech.* **274**, 219–241.

KERSWELL, R. R. 1994*b* Elliptical instabilities of stratified, hydromagnetic waves. *Geophys. Astrophys. Fluid Dyn.* (In press).

PROCTOR, M. R. E. 1994 Magnetoconvection in a rapidly rotating sphere. In *Stellar and Planetary Dynamos* (ed. M. R. E. Proctor & A. D. Gilbert), Cambridge University Press.

ROBERTS, P. H. 1968 On the thermal instability of a self-gravitating fluid sphere containing heat sources. *Phil. Trans. R. Soc. Lond.* A **263**, 93–117.

SOWARD, A. M. 1977 On the finite amplitude thermal instability of a rapidly rotating fluid sphere. *Geophys. Astrophys. Fluid Dyn.* **9**, 19–74.

STEWARTSON, K. 1966 On almost rigid rotations. *J. Fluid Mech.* **26**, 131–144.

YANO, J.-I. 1992 Asymptotic theory of thermal convection in the rapidly rotating systems. *J. Fluid Mech.* **243**, 103–131.

ZHANG, K. 1992 Spiralling columnar convection in rapidly rotating spherical fluid shells. *J. Fluid Mech.* **236**, 535–556.

ZHANG, K. 1993 On equatorially trapped boundary inertial waves. *J. Fluid Mech.* **248**, 203–217.

ZHANG, K. 1994 On coupling between the Poincaré equation and the heat equation. *J. Fluid Mech.* **268**, 211–229.

ZHANG, K. & BUSSE, F. 1987 On the onset of convection in rotating spherical shells. *Geophys. Astrophys. Fluid Dyn.* **39**, 119–147.